ASME Journal of Applied Mechanics
Online journal at:
https://asmedigitalcollection.asme.org/appliedmechanics

Ihina Mahajan
Material Science and Engineering Program,
University of Houston,
Houston, TX 77024
e-mail: imahaja2@cougarnet.uh.edu

Pratik Khandagale
Los Alamos National Laboratory,
Los Alamos, NM 87545
e-mail: pkhandag@alumni.cmu.edu

Liping Liu[1]
Department of Mathematics,
Rutgers University,
New Brunswick, NJ 08854
e-mail: liu.liping@rutgers.edu

Pradeep Sharma[1]
Department of Physics,
University of Houston,
Houston, TX 77204
e-mail: psharma@central.uh.edu

Fluctuation-Induced Electromechanical Transitions in Active Cell Aggregates

Living tissues are fundamentally distinct from passive matter; they generate internal forces, sustain autonomous flows, and communicate through complex electrical signaling. While these active processes drive the nonequilibrium fluctuations that shape tissue mechanics, the impact of this "active noise" on electromechanical coupling remains poorly understood. While fluctuations in active cell membranes have been extensively studied, a comparable theoretical understanding at the tissue scale remains elusive. In this study, we propose a coarse-grained theoretical framework that integrates thermal and active noise into a unified electromechanical field theory for cell aggregates. By applying Langevin dynamics, we derive the fluctuation spectrum of shear strain and demonstrate that cellular activity fundamentally renormalizes the tissue's elastic and electromechanical properties. Our model shows that active fluctuations can soften tissue stiffness and couple nonlinearly with electrical potential, triggering activity-driven shifts in phase behavior. These results suggest that active noise is an important driver of electromechanical state changes, potentially offering a mechanistic lens through which to view morphogenesis, mechanosensation, and bioelectric patterning. [DOI: 10.1115/1.4071367]

Keywords: cell aggregate, electromechanical coupling, solid-to-fluid phase transition, nonequilibrium statistical mechanics, computational mechanics, constitutive modeling of materials

1 Introduction

Living tissues are fundamentally distinct from passive structural materials, operating as dynamic systems of cells that continuously consume energy to move, deform, and generate internal forces as they interact with their environment. Biological systems, therefore, belong to the broader class of active matter operating far from equilibrium. A general overview of the continuum and statistical-mechanical approaches to active biological matter can be found in [1]. Rather than behaving as inert structural elements, these cells maintain steep ion concentration gradients and actively remodel their internal cytoskeleton through complex, ATP-driven processes [2,3]. This sustained metabolic activity fosters a remarkable state in which mechanical action and electrical polarization are not merely coexistent, but are profoundly and dynamically intertwined.

For instance, mechanical deformations such as the stretching of a cell membrane can activate mechanosensitive ion channels to modulate membrane potential [4,5], while changes in voltage can conversely reorganize cytoskeletal networks and alter cellular tension [6,7]. Direct evidence of this coupling has been observed in experiments combining patch-clamp recordings with atomic force microscopy, which reveal that voltage fluctuations can induce immediate changes in membrane shape [8,9]. Ultimately, this reciprocal feedback loop lies at the heart of cellular mechanotransduction, enabling cells to efficiently convert physical environmental cues into coordinated biochemical and electrical signals [10]

When these individual cells act in concert within a tissue, their collective dynamics give rise to emergent behaviors that transcend the properties of any single cell. Tissues possess the remarkable capacity to flow, jam, fold, or undergo abrupt morphological transitions—often driven by internal active stresses rather than external mechanical loads [11,12]. These transitions are fundamental to critical biological processes, including embryonic development, wound healing, and tumor invasion, where cell populations move and deform in a coordinated yet intrinsically stochastic manner [13,14].

Recent experimental evidence highlights that tissues maintain large, persistent fluctuations in both deformation and membrane potential even in a quiescent state. For instance, time-resolved traction force microscopy and mechanical wave propagation assays have demonstrated that epithelial monolayers generate spontaneous force fluctuations across long-range scales [15,16]. Similarly, the "flickering" observed in red blood cell membranes has been identified as an active process driven by adenosine triphosphate (ATP) rather than a simple thermal equilibrium effect [17]. These fluctuations are significantly larger than those predicted by thermal noise alone, suggesting a deeply nonequilibrium origin rooted in active cellular processes [17,18].

What fundamentally drives these nonequilibrium fluctuations and how do they redefine the physical state of a tissue? Internally, cells generate fluctuating forces through actomyosin contractions, ion transport, and stochastic motor activity, all of which break

[1]Corresponding authors.

Manuscript received February 8, 2026; final manuscript received March 8, 2026; published online July 28, 2026. Tech. Editor: Yonggang Huang.

detailed balance and inject energy at the microscale [19]. These active fluctuations can produce dramatic effects; for instance, in epithelial monolayers, increased activity or confinement can fluidize the tissue and drive an unjamming transition even in the absence of gene-level changes associated with epithelial–mesenchymal transition [20]. Experiments with synthetic or reconstituted tissue systems further demonstrate that internal fluctuations and geometric constraints alone can lead to rigidity breakdown even without biochemical regulation [21,22]. Collectively, these findings suggest that fluctuations are not simply noise; instead, they can act as control parameters that restructure a tissue's electromechanical state (Fig. 1).

Several theoretical models have addressed fragments of this problem. The classical Helfrich model describes membrane undulations via curvature elasticity under thermal fluctuations [23]. This framework has been used extensively to model shape fluctuations in lipid vesicles and red blood cells [24,25]. Extensions of this model incorporate active-noise and nonlinear curvature effects, as shown in recent work [26], by Kulkarni who demonstrated that active fluctuations renormalize membrane stiffness and generate correlated fluctuations. Similar renormalization of effective mechanical properties in fluctuating active membranes has also been reported in recent analytical studies [27]. These ideas have also been used to explain how vesicle size distributions may change when compared with equilibrium calculations [28–32], or how sensitively electrical fields can be detected. Active matter theories, such as vertex-based models and continuum active gels, describe collective tissue mechanics including emergent rigidity transitions and flows [11,18]. Flexoelectric models provide a separate framework for coupling strain gradients and polarization in biological systems and have been validated in synthetic lipid systems and membranes [33–35]. However, most of these frameworks either neglect the coupling between strain and voltage or rely on equilibrium assumptions that exclude the role of active, stochastic fluctuations.

In this work, we develop a continuum theory of living cell aggregates that captures the stochastic electromechanical dynamics arising from both thermal and active fluctuations at steady-state. Our formulation draws on foundational developments in elastic membrane mechanics [23,36] and the statistical thermodynamics of fluctuating soft interfaces. In addition, statistical field theory and coarse-graining frameworks developed for nonlinear soft materials [37–39] provide a methodological foundation for systematically deriving fluctuation-renormalized material properties. Building on these approaches, and extending recent statistical-mechanical treatments of cell aggregates [40], we construct a unified description of strain–voltage coupling in active tissues.

The model couples mechanical strain and membrane potential through a nonlinear energy functional and derives their dynamics via Langevin equations with distinct thermal and active-noise sources. By analytically computing the resulting fluctuation spectrum, we demonstrate that active fluctuations renormalize the effective mechanical stiffness, shift the equilibrium membrane potential, and can induce a fluctuation-driven transition from a solid-like to a fluid-like state. These results provide a mechanistic basis for experimentally observed tissue fluidization, electromechanical remodeling, and activity-induced rigidity transitions in both living and synthetic systems. More broadly, the framework clarifies how nonequilibrium fluctuations can fundamentally reshape material properties in active biological matter and suggests design principles for responsive, fluctuation-driven materials.

The rest of this paper is organized as follows. In Sec. 2, we present the theoretical model, introducing the Hamiltonian and deriving the Langevin equations that govern the time evolution of the strain and potential fields. In Sec. 3, we compute the fluctuation spectrum under both thermal and active noise and use it to derive effective free energy and material parameters. Section 4 discusses the physical implications of our results, including renormalized resting potential, activity-induced phase transitions, and nonlinear electromechanical response using biologically relevant parameters. Finally, in Sec. 5, we summarize our findings.

2 Theoretical Formulation

2.1 Phenomenological Continuum Model. We model a living cell aggregate as a collection of N mechanically and electrically interacting cells. Each cell can deform and exhibit variations in its transmembrane potential. The mechanical state of the ith cell is represented by a *symmetric strain tensor* $\mathbf{E}_i \in \mathbb{R}^{2\times2}_{\text{sym}}$ whereas the electrical state is represented by a transmembrane potential ξ_i. To encode incompressibility, we impose $tr\mathbf{E}_i = 0$. Thus, the electromechanical state of the ith cell is described by the pair $(\mathbf{E}_i, \xi_i)$. The admissible state space for a single cell is

$$\mathcal{D} := \left\{(\mathbf{E}, \xi) \in \mathbb{R}^{2\times2}_{\text{sym}} \times \mathbb{R} : tr\mathbf{E} = 0\right\}, \qquad i = 1, 2, \ldots, N \tag{1}$$

To describe the electromechanical properties of the cell aggregate, we postulate a single-cell energy function that accounts for mechanical strain, transmembrane potential, and their electromechanical coupling [40]:

$$\psi(\mathbf{E}, \xi) = \left(\frac{\mu}{\gamma^{*2}}|\mathbf{E}|^2(|\mathbf{E}|^2 - \gamma^*)^2 + \frac{\epsilon}{2\lambda^2}(\xi - \xi^*)^2 + K(\xi - \xi^*)|\mathbf{E}|^2\right)A \tag{2}$$

where A denotes the in-plane area per cell (with unit thickness, A is also the cell volume). The first term, $(\mu/\gamma^{*2})\,|\mathbf{E}|^2\left(|\mathbf{E}|^2 - \gamma^*\right)^2$, accounts for the strain energy: the shear modulus $\mu > 0$ quantifies the cell's resistance to shear, and γ^* reflects alternative ground-energy celluar arrangement in T1 transition [41]. The second term, $(\epsilon/2\lambda^2)(\xi - \xi^*)^2$, represents the electrical energy stored in the membrane, where ξ^* is the resting potential, ϵ is an effective dielectric parameter, and λ is a length scale comparable to the membrane thickness. The last term, $K(\xi - \xi^*)|\mathbf{E}|^2$, encodes the electromechanical coupling with strength K.

We incorporate nearest–neighbor interactions to account for mechanical and electrical coupling between cells in the aggregate. For the ith cell, we postulate the interaction energy [40]:

$$H^{(i)}_{\text{int}}(\mathbf{E}_i, \xi_i) = \frac{A}{2\,l^2}\left(J^{\text{elas}}\sum_{j\in\mathcal{I}_i}|\mathbf{E}_i - \mathbf{E}_j|^2 + J^{\text{elec}}\sum_{j\in\mathcal{I}_i}|\xi_i - \xi_j|^2\right) \tag{3}$$

where $\mathcal{I}_i$ is the set of nearest neighbors of cell i, l is a length scale comparable to the cell size, and J^{elas}, $J^{\text{elec}} > 0$ are coupling constants for mechanical and electrical interactions, respectively. The factor $1/2$ avoids double counting of pairwise interactions. The Hamiltonian of the N cell aggregate system is then given by

$$H(\{\mathbf{E}_i, \xi_i\}_{i=1}^N) = \sum_{i=1}^N \psi(\mathbf{E}_i, \xi_i) + \sum_{i=1}^N H^{(i)}_{\text{int}}(\mathbf{E}_i, \xi_i) \tag{4}$$

To pass to a continuum description, we introduce smoothly varying fields $\mathbf{E}(\mathbf{r})$ and $\xi(\mathbf{r})$ and approximate nearest–neighbor differences by gradient terms:

$$\sum_{j\in\mathcal{I}_i}|\mathbf{E}_i - \mathbf{E}_j|^2 \longrightarrow l^2\,|\nabla\mathbf{E}(\mathbf{r})|^2, \qquad \sum_{j\in\mathcal{I}_i}|\xi_i - \xi_j|^2 \longrightarrow l^2\,|\nabla\xi(\mathbf{r})|^2 \tag{5}$$

where $\mathbf{r} = (x, y)$ denotes position on the membrane patch. Replacing the sum over cells in Eq. (4) by an integral, $\sum A \to \int d\mathbf{r}$, yields

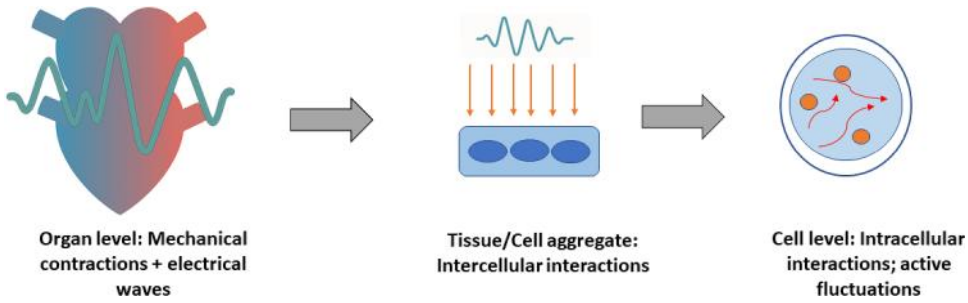

Fig. 1 Schematic overview illustrating multiscale electromechanical interactions: from organ-level waves, through tissue aggregates and intercellular coupling, to intracellular active fluctuations

the Hamiltonian of the continuum model:

$$H[\mathbf{E},\xi]=\int d\mathbf{r}\left(\frac{\mu}{\gamma^{*2}}|\mathbf{E}|^2\left(|\mathbf{E}|^2-\gamma^*\right)^2+\frac{\epsilon}{2\lambda^2}(\xi-\xi^*)^2 +K(\xi-\xi^*)|\mathbf{E}|^2+\tfrac{1}{2}J^{\text{elas}}|\nabla\mathbf{E}|^2+\tfrac{1}{2}J^{\text{elec}}|\nabla\xi|^2\right) \tag{6}$$

To simplify the analysis while retaining the essential features of the mechanical deformations, we project the strain tensor $\mathbf{E}\in\mathbb{R}^{2\times2}_{\text{sym}}$ onto a single variable γ, representing pure shear strain as

$$\mathbf{E}=\begin{bmatrix}0&\gamma\\ \gamma&0\end{bmatrix},\quad |\mathbf{E}|^2=2\gamma^2 \tag{7}$$

Using the scalar representation of strain $\mathbf{E}(\mathbf{r})\to\gamma(\mathbf{r})$, the Hamiltonian (6) can be rewritten as

$$H[\gamma,\xi]=\int d\mathbf{r}\left(\frac{\mu}{\gamma^{*2}}2\gamma^2(2\gamma^2-\gamma^*)^2+\frac{\epsilon}{2\lambda^2}(\xi-\xi^*)^2+K(\xi-\xi^*)2\gamma^2+J^{\text{elas}}|\nabla\gamma|^2+\frac{1}{2}J^{\text{elec}}|\nabla\xi|^2\right) \tag{8}$$

The Hamiltonian (8) is anharmonic in strain. To facilitate fluctuation analysis, we expand and truncate the Hamiltonian around an equilibrium state. Let $(\bar\gamma,\bar\xi)$ denote the averages of strain and potential, and (γ',ξ') denote fluctuations defined by

$$(\gamma',\xi')=(\gamma,\xi)-(\bar\gamma,\bar\xi) \tag{9}$$

To obtain a harmonic model for the fluctuations (γ',ξ'), we expand the Hamiltonian (8) about the average state $(\bar\gamma,\bar\xi)$ and retain only terms up to second order as follows. In particular, the nonlinear mechanical energy density can be approximated as

$$\begin{aligned}f_1(\gamma)&\approx f_1(\bar\gamma)+\frac{\partial}{\partial\gamma}f_1(\gamma)|_{\bar\gamma}\gamma'+\frac{\partial^2}{\partial\gamma^2}f_1(\gamma)|_{\bar\gamma}\gamma'^2\\ &=C_1+L_1\gamma'+Q_1\gamma'^2\end{aligned}$$

where

$$\begin{aligned}C_1&=\frac{2\mu}{\gamma^{*2}}\bar\gamma^2(2\bar\gamma^2-\gamma^*)^2 \quad \text{Constantterm}\\ L_1&=\frac{2\mu}{\gamma^{*2}}(2\bar\gamma(12\bar\gamma^4-8\bar\gamma^2\gamma^*+\gamma^{*2})) \quad \text{Linearcoefficient}\\ Q_1&=\frac{4\mu}{\gamma^{*2}}(60\bar\gamma^4-24\bar\gamma^2\gamma^*+\gamma^{*2}) \quad \text{Quadraticcoefficient}\end{aligned} \tag{10}$$

Similarly, the electrical potential energy expands as

$$\begin{aligned}f_2(\xi)&=\frac{\epsilon}{2\lambda^2}(\xi-\xi^*)^2=\frac{\epsilon}{2\lambda^2}(\bar\xi-\xi^*+\xi')^2\\ &=\frac{\epsilon}{2\lambda^2}[(\bar\xi-\xi^*)^2+\xi'^2+2(\bar\xi-\xi^*)\xi')]\end{aligned}$$

The coupling term gives rise to

$$\begin{aligned}f_3(\gamma,\xi)&=2K(\bar\gamma^2+\gamma'^2+2\bar\gamma\gamma')(\bar\xi-\xi^*+\xi')\\ &=2K[2\bar\gamma^2(\bar\xi-\xi^*)+2\bar\gamma^2\xi'+2\bar\gamma(\bar\xi-\xi^*)\gamma'+(2\bar\gamma)\gamma'\xi'+\gamma'^2\xi'^2]\end{aligned}$$

Suppose that the averages $\bar\gamma$ and $\bar\xi$ are spatially uniform, and hence

$$J^{\text{elas}}|\nabla\gamma|^2=J^{\text{elas}}|\nabla\gamma'|^2,\qquad J^{\text{elec}}|\nabla\xi|^2=J^{\text{elec}}|\nabla\xi'|^2$$

For brevity, we subsequently drop the primes ($'$), denote the fluctuating fields by γ and ξ, and collect the fluctuations into the state vector

$$\boldsymbol{\phi}:=\begin{bmatrix}\gamma\\ \xi\end{bmatrix} \tag{11}$$

Neglecting the constant and linear terms, we obtain the harmonic Hamiltonian for fluctuations in real space as

$$\begin{aligned}&H[\boldsymbol{\phi}]\\ &=\int d\mathbf{r}\left(Q_1\gamma^2+\frac{\epsilon}{2\lambda^2}\xi^2+(4K\bar\gamma)\gamma\xi+J^{\text{elas}}|\nabla\gamma|^2+\frac{1}{2}J^{\text{elec}}|\nabla\xi|^2\right)\end{aligned} \tag{12}$$

where Q_1 is given in Eq. (10).

To analyze spatial fluctuations, we transform the Hamiltonian to Fourier space using inverse Fourier transform identities:

$$\begin{aligned}\gamma(\mathbf{r})&=\int\frac{d\mathbf{q}}{(2\pi)^d}e^{i\mathbf{q}\cdot\mathbf{r}}\gamma_{\mathbf{q}},\quad \xi(\mathbf{r})=\int\frac{d\mathbf{q}}{(2\pi)^d}e^{i\mathbf{q}\cdot\mathbf{r}}\xi_{\mathbf{q}}\\ |\nabla\gamma(\mathbf{r})|^2&=\int\frac{d\mathbf{q}}{(2\pi)^d}q^2|\gamma_{\mathbf{q}}|^2,\quad |\nabla\xi(\mathbf{r})|^2=\int\frac{d\mathbf{q}}{(2\pi)^d}q^2|\xi_{\mathbf{q}}|^2\end{aligned} \tag{13}$$

where $d=2$ is the dimension of the physical space, and we define $q:=|\mathbf{q}|$. By Parseval's theorem, we can rewrite the Hamiltonian in

Eq. (12) in $\mathbf{q}$-space as

$$H_{\mathbf{q}} = Q_1 |\gamma_{\mathbf{q}}|^2 + \frac{\epsilon}{2\lambda^2} |\xi_{\mathbf{q}}|^2 + 4K\bar{\gamma}\gamma_{\mathbf{q}}\xi_{\mathbf{q}} + q^2 J^{\text{elas}} |\gamma_{\mathbf{q}}|^2 + \frac{1}{2} J^{\text{elec}} q^2 |\xi_{\mathbf{q}}|^2 =: \frac{1}{2} \boldsymbol{\phi}_{\mathbf{q}}^{\dagger} \mathbf{M}_{\mathbf{q}} \boldsymbol{\phi}_{\mathbf{q}} \tag{14}$$

where the superscript † denotes the conjugate transpose and

$$\mathbf{M}_{\mathbf{q}} = \begin{bmatrix} 2(Q_1 + q^2 J^{\text{elas}}) & 4K\bar{\gamma} \\ 4K\bar{\gamma} & \frac{\epsilon}{\lambda^2} + q^2 J^{\text{elec}} \end{bmatrix}, \quad \boldsymbol{\phi}_{\mathbf{q}} = \begin{bmatrix} \gamma_{\mathbf{q}} \\ \xi_{\mathbf{q}} \end{bmatrix} \tag{15}$$

3 Time Evolution of a Living Cell Aggregate

To model the nonequilibrium dynamics of an active cell aggregate, we consider the stochastic evolution of the state variables. Accounting for both thermal and active noise, the time evolution of fluctuations $\boldsymbol{\phi}(\mathbf{r}, t)$ can be modeled by an overdamped Langevin equation [26]:

$$\frac{\partial \boldsymbol{\phi}}{\partial t}(\mathbf{r}, t) = \int_{\mathbb{R}^2} \boldsymbol{\Lambda}(\mathbf{r} - \mathbf{r}') \left[-\frac{\delta H}{\delta \boldsymbol{\phi}}(\mathbf{r}', t) + \boldsymbol{\eta}^{\text{th}}(\mathbf{r}', t) + \boldsymbol{\eta}^{\text{a}}(\mathbf{r}', t) \right] d\mathbf{r}' \tag{16}$$

where $H[\boldsymbol{\phi}]$ is the quadratic Hamiltonian from Eq. (12), the (Fréchet) functional derivative $-\frac{\delta H}{\delta \boldsymbol{\phi}}(\mathbf{r}', t)$ can be interpreted as the local generalized force, $\boldsymbol{\Lambda}(\mathbf{r})$ is the mobility kernel, and $\boldsymbol{\eta}^{\text{th}}$ and $\boldsymbol{\eta}^{\text{a}}$ denote the thermal and active-noise fields, respectively. By calculus of variation and Eq. (12), we find the functional derivative of the Hamiltonian as

$$\frac{\delta H}{\delta \boldsymbol{\phi}} = \begin{bmatrix} \frac{\delta H}{\delta \gamma} \\ \frac{\delta H}{\delta \xi} \end{bmatrix} = \begin{bmatrix} 2Q_1 \gamma + 4K\bar{\gamma}\xi - 2J^{\text{elas}} \Delta\gamma \\ \frac{\epsilon}{\lambda^2} \xi + 4K\bar{\gamma}\gamma - J^{\text{elec}} \Delta\xi \end{bmatrix} \tag{17}$$

For simplicity, assume that the mobility kernel $\boldsymbol{\Lambda}(\mathbf{r}) = \text{diag}[\Lambda^{\gamma}(\mathbf{r}), \Lambda^{\xi}(\mathbf{r})]$ is diagonal. Applying spatial Fourier transform $f(\mathbf{r}) \mapsto f_{\mathbf{q}} = \int f(\mathbf{r}) e^{-i\mathbf{q}\cdot\mathbf{r}} d\mathbf{r}$ to (16) yields a linear stochastic ODE for each mode $\boldsymbol{\phi}_{\mathbf{q}}(t)$

$$\frac{\partial \boldsymbol{\phi}_{\mathbf{q}}}{\partial t} = \boldsymbol{\Theta}_{\mathbf{q}} \boldsymbol{\phi}_{\mathbf{q}} + \mathbf{F}^{\text{th}}_{\mathbf{q}}(t) + \mathbf{F}^{\text{a}}_{\mathbf{q}}(t) \tag{18}$$

and

$$\boldsymbol{\Theta}_{\mathbf{q}} = \begin{bmatrix} -\Lambda^{\gamma}_{\mathbf{q}} \left(2Q_1 + 2J^{\text{elas}} q^2 \right) & -\Lambda^{\gamma}_{\mathbf{q}} (4K\bar{\gamma}) \\ -\Lambda^{\xi}_{\mathbf{q}} (4K\bar{\gamma}) & -\Lambda^{\xi}_{\mathbf{q}} \left(\frac{\epsilon}{\lambda^2} + J^{\text{elec}} q^2 \right) \end{bmatrix} \tag{19}$$

and the noise–force vectors

$$\mathbf{F}^{\text{th}}_{\mathbf{q}}(t) = \begin{bmatrix} \Lambda^{\gamma}_{\mathbf{q}} (\eta^{\text{th}}_{\mathbf{q}})^{\gamma}(t) \\ \Lambda^{\xi}_{\mathbf{q}} (\eta^{\text{th}}_{\mathbf{q}})^{\xi}(t) \end{bmatrix}, \quad \mathbf{F}^{\text{a}}_{\mathbf{q}}(t) = \begin{bmatrix} \Lambda^{\gamma}_{\mathbf{q}} (\eta^{\text{a}}_{\mathbf{q}})^{\gamma}(t) \\ \Lambda^{\xi}_{\mathbf{q}} (\eta^{\text{a}}_{\mathbf{q}})^{\xi}(t) \end{bmatrix} \tag{20}$$

Here, $\Lambda^{\gamma}_{\mathbf{q}}$ and $\Lambda^{\xi}_{\mathbf{q}}$ denote the Fourier symbols of the mobility kernel for the γ and ξ components, respectively. Quantities $(\eta^{\text{th}}_{\mathbf{q}})^{\gamma}$, $(\eta^{\text{a}}_{\mathbf{q}})^{\gamma}$ are Fourier modes of thermal and active noise, respectively, for γ component, whereas $(\eta^{\text{th}}_{\mathbf{q}})^{\xi}$, $(\eta^{\text{a}}_{\mathbf{q}})^{\xi}$ are Fourier modes of thermal and active noise, respectively, for ξ component, and $\Delta \to -q^2$ under the Fourier transform.

3.1 Fluctuation Analysis

3.1.1 Fluctuation Spectrum With Thermal Noise. In the presence of *only* thermal noise, Eq. (18) reduces to

$$\frac{\partial \boldsymbol{\phi}_{\mathbf{q}}(t)}{\partial t} = \boldsymbol{\Theta}_{\mathbf{q}} \boldsymbol{\phi}_{\mathbf{q}}(t) + \mathbf{F}^{\text{th}}_{\mathbf{q}}(t) \tag{21}$$

Assume that the thermal noises are uncorrelated across Fourier modes and satisfy

$$\left\langle \mathbf{F}^{\text{th}}_{\mathbf{q}}(t) \, \mathbf{F}^{\text{th}}_{\mathbf{q}'}(t')^{\top} \right\rangle = 2 \, \mathbf{B}^{\text{th}}_{\mathbf{q}} \delta_{\mathbf{q}\mathbf{q}'} \, \delta(t - t') \tag{22}$$

where $\mathbf{B}^{\text{th}}_{\mathbf{q}}$ is a symmetric, positive semidefinite 2×2 matrix measuring the strength of thermal noises. For consistency with the fluctuation–dissipation theorem, the stochastic differential equation (SDE) (Eqs. (21)–(22)) implies that [19]

$$\mathbf{B}^{\text{th}}_{\mathbf{q}} = -\frac{1}{2} \left(\boldsymbol{\Theta}_{\mathbf{q}} \, \mathbf{P}^{\text{th}}_{\mathbf{q}} + \mathbf{P}^{\text{th}}_{\mathbf{q}} \, \boldsymbol{\Theta}^{\top}_{\mathbf{q}} \right) \tag{23}$$

where $\mathbf{P}^{\text{th}}_{\mathbf{q}}$ is the (equilibrium) fluctuation spectrum, i.e., the covariance of the Fourier modes at equilibrium under thermal noise only:

$$\mathbf{P}^{\text{th}}_{\mathbf{q}} := \left\langle \boldsymbol{\phi}_{\mathbf{q}}(t) \otimes \boldsymbol{\phi}_{\mathbf{q}}(t) \right\rangle^{\text{th}}_{\text{eq}} = \begin{bmatrix} \left\langle |\gamma_{\mathbf{q}}|^2 \right\rangle^{\text{th}}_{\text{eq}} & \left\langle \gamma_{\mathbf{q}} \, \xi_{\mathbf{q}} \right\rangle^{\text{th}}_{\text{eq}} \\ \left\langle \gamma_{\mathbf{q}} \, \xi_{\mathbf{q}} \right\rangle^{\text{th}}_{\text{eq}} & \left\langle |\xi_{\mathbf{q}}|^2 \right\rangle^{\text{th}}_{\text{eq}} \end{bmatrix} \tag{24}$$

At constant temperature T, the equipartition theorem yields [35]

$$\left\langle (\phi_{\mathbf{q}})_i (\phi^*_{\mathbf{q}})_j \right\rangle^{\text{th}} = \frac{k_B T}{L^3} \left[\mathbf{M}^{-1}_{\mathbf{q}} \right]_{ij} \tag{25}$$

where $\mathbf{M}_{\mathbf{q}}$ is the 2×2 matrix defined in Eqs. (14)–(15). More specifically, upon inverting the matrix $\mathbf{M}_{\mathbf{q}}$ we find the components of Eq. (24) as

$$\begin{aligned} \left\langle |\gamma_{\mathbf{q}}|^2 \right\rangle^{\text{th}}_{\text{eq}} &= \frac{k_B T L^3 \left(\frac{\epsilon}{\lambda^2} + J^{\text{elec}} q^2 \right)}{\left(2Q_1 + 2J^{\text{elas}} q^2 \right) \left(\frac{\epsilon}{\lambda^2} + J^{\text{elec}} q^2 \right) - 16K^2 \bar{\gamma}^2} \\ \left\langle \gamma_{\mathbf{q}} \xi_{\mathbf{q}} \right\rangle^{\text{th}}_{\text{eq}} &= -\frac{k_B T L^3 4K\bar{\gamma}}{\left(2Q_1 + 2J^{\text{elas}} q^2 \right) \left(\frac{\epsilon}{\lambda^2} + J^{\text{elec}} q^2 \right) - 16K^2 \bar{\gamma}^2} \\ \left\langle |\xi_{\mathbf{q}}|^2 \right\rangle^{\text{th}}_{\text{eq}} &= \frac{k_B T L^3 \left(2Q_1 + 2J^{\text{elas}} q^2 \right)}{\left(2Q_1 + 2J^{\text{elas}} q^2 \right) \left(\frac{\epsilon}{\lambda^2} + J^{\text{elec}} q^2 \right) - 16K^2 \bar{\gamma}^2} \end{aligned} \tag{26}$$

Derivation of Eq. (23). The technical details for arriving at Eq. (23) are as follows. Solving the linear SDE (21) for thermal noise only and neglecting the decaying term from $\boldsymbol{\phi}_{\mathbf{q}}(0)$, we obtain

$$\boldsymbol{\phi}_{\mathbf{q}}(t) = \int_0^t e^{(t-s)\boldsymbol{\Theta}_{\mathbf{q}}} \, \mathbf{F}^{\text{th}}_{\mathbf{q}}(s) \, ds$$

Hence, the covariance

$$\begin{aligned} \left\langle \boldsymbol{\phi}_{\mathbf{q}}(t) \otimes \boldsymbol{\phi}_{\mathbf{q}}(t) \right\rangle^{\text{th}} &= \int_0^t \int_0^t e^{(t-s)\boldsymbol{\Theta}_{\mathbf{q}}} 2\mathbf{B}^{\text{th}}_{\mathbf{q}} \, \delta(s - s') e^{(t-s')\boldsymbol{\Theta}^{\top}_{\mathbf{q}}} \, ds \, ds' \\ &= 2 \int_0^t e^{\tau\boldsymbol{\Theta}_{\mathbf{q}}} \mathbf{B}^{\text{th}}_{\mathbf{q}} e^{\tau\boldsymbol{\Theta}^{\top}_{\mathbf{q}}} \, d\tau \end{aligned}$$

where $\tau = (t - s)$.

At stationary ($t \to \infty$),

$$\mathbf{P}^{\text{th}}_{\mathbf{q}} = \left\langle \boldsymbol{\phi}_{\mathbf{q}}(t) \otimes \boldsymbol{\phi}_{\mathbf{q}}(t) \right\rangle^{\text{th}}_{\text{eq}} = 2 \int_0^{\infty} e^{\tau\boldsymbol{\Theta}_{\mathbf{q}}} \mathbf{B}^{\text{th}}_{\mathbf{q}} e^{\tau\boldsymbol{\Theta}^{\top}_{\mathbf{q}}} d\tau \tag{27}$$

Differentiating the integrand with respect to τ and then integrating over $(0, +\infty)$, we conclude that (27) satisfies the Sylvester/Lyapunov equation [42]

$$\boldsymbol{\Theta}_{\mathbf{q}} \mathbf{P}^{\text{th}}_{\mathbf{q}} + \mathbf{P}^{\text{th}}_{\mathbf{q}} \boldsymbol{\Theta}^{\top}_{\mathbf{q}} = 2 \left[e^{\tau\boldsymbol{\Theta}_{\mathbf{q}}} \mathbf{B}^{\text{th}}_{\mathbf{q}} e^{\tau\boldsymbol{\Theta}^{\top}_{\mathbf{q}}} \right]^{\infty}_{\tau=0} = -2\mathbf{B}^{\text{th}}_{\mathbf{q}} \tag{28}$$

which is equivalent to Eq. (23).

3.1.2 Fluctuation Spectrum With Both Thermal and Active Noise. With both thermal and active noise present, Eq. (18)

becomes

$$\frac{\partial \boldsymbol{\phi}_{\mathbf{q}}(t)}{\partial t} = \boldsymbol{\Theta}_{\mathbf{q}}\,\boldsymbol{\phi}_{\mathbf{q}}(t) + \mathbf{F}^{\mathrm{th}}_{\mathbf{q}}(t) + \mathbf{F}^{\mathrm{a}}_{\mathbf{q}}(t) \tag{29}$$

We model the active noise as zero-mean, exponentially correlated (Ornstein–Uhlenbeck) and diagonal in the (γ, ξ) components:

$$\begin{aligned} \left\langle \boldsymbol{\eta}^{\mathrm{a}}_{\mathbf{q}}(t) \otimes \boldsymbol{\eta}^{\mathrm{a}}_{\mathbf{q}'}(t') \right\rangle &= \boldsymbol{\Gamma}^{\mathrm{a}}_{\mathbf{q}}\, e^{-|t-t'|/\tau_a}\, \delta_{\mathbf{q}\mathbf{q}'}, \\ \boldsymbol{\Gamma}^{\mathrm{a}}_{\mathbf{q}} &= \begin{bmatrix} (\Gamma^{\mathrm{a}}_{\mathbf{q}})^{\gamma} & 0 \\ 0 & (\Gamma^{\mathrm{a}}_{\mathbf{q}})^{\xi} \end{bmatrix} \end{aligned} \tag{30}$$

where $\tau_a > 0$ is the correlation time scale for active noise, and $(\Gamma^{\mathrm{a}}_{\mathbf{q}})^{\gamma}$, $(\Gamma^{\mathrm{a}}_{\mathbf{q}})^{\xi}$ set the active-noise strengths of the strain and potential components, respectively.

Using Eqs. (20) and (30), and assuming the γ and ξ components of the active noise are uncorrelated, the active force covariance is

$$\begin{aligned} &\left\langle \mathbf{F}^{\mathrm{a}}_{\mathbf{q}}(t) \otimes \mathbf{F}^{\mathrm{a}}_{\mathbf{q}'}(t') \right\rangle \\ &= \begin{bmatrix} \left(\Lambda^{\gamma}_{\mathbf{q}}\right)^2 \left\langle (\eta^{\mathrm{a}}_{\mathbf{q}})^{\gamma}(t)\, (\eta^{\mathrm{a}}_{\mathbf{q}'})^{\gamma}(t') \right\rangle & 0 \\ 0 & \left(\Lambda^{\xi}_{\mathbf{q}}\right)^2 \left\langle (\eta^{\mathrm{a}}_{\mathbf{q}})^{\xi}(t)\, (\eta^{\mathrm{a}}_{\mathbf{q}'})^{\xi}(t') \right\rangle \end{bmatrix} \\ &= 2\,\mathbf{B}^{\mathrm{a}}_{\mathbf{q}}\, e^{-|t-t'|/\tau_a}\, \delta_{\mathbf{q}\mathbf{q}'}, \end{aligned} \tag{31}$$

with diagonal, symmetric

$$\mathbf{B}^{\mathrm{a}}_{\mathbf{q}} = \frac{1}{2} \begin{bmatrix} \left(\Lambda^{\gamma}_{\mathbf{q}}\right)^2 (\Gamma^{\mathrm{a}}_{\mathbf{q}})^{\gamma} & 0 \\ 0 & \left(\Lambda^{\xi}_{\mathbf{q}}\right)^2 (\Gamma^{\mathrm{a}}_{\mathbf{q}})^{\xi} \end{bmatrix} \tag{32}$$

Neglecting the decaying term from $\boldsymbol{\phi}_{\mathbf{q}}(0)$, the solution of Eq. (18) is given by

$$\boldsymbol{\phi}_{\mathbf{q}}(t) = \int_0^t e^{(t-s)\boldsymbol{\Theta}_{\mathbf{q}}} \left(\mathbf{F}^{\mathrm{th}}_{\mathbf{q}}(s) + \mathbf{F}^{\mathrm{a}}_{\mathbf{q}}(s) \right) ds \tag{33}$$

Assume that $\mathbf{F}^{\mathrm{th}}_{\mathbf{q}}$ and $\mathbf{F}^{\mathrm{a}}_{\mathbf{q}}$ are mutually uncorrelated. The covariance splits additively:

$$\begin{aligned} &\left\langle \boldsymbol{\phi}_{\mathbf{q}}(t) \otimes \boldsymbol{\phi}_{\mathbf{q}}(t) \right\rangle^{\mathrm{th,a}} \\ &= \int_0^t \int_0^t e^{(t-s)\boldsymbol{\Theta}_{\mathbf{q}}} \left(2\mathbf{B}^{\mathrm{th}}_{\mathbf{q}}\, \delta(s-s') + 2\mathbf{B}^{\mathrm{a}}_{\mathbf{q}}\, e^{-|s-s'|/\tau_a} \right) e^{(t-s')\boldsymbol{\Theta}^{\top}_{\mathbf{q}}}\, ds\, ds' \\ &= \underbrace{2\int_0^t e^{(t-s)\boldsymbol{\Theta}_{\mathbf{q}}} \mathbf{B}^{\mathrm{th}}_{\mathbf{q}} e^{(t-s)\boldsymbol{\Theta}^{\top}_{\mathbf{q}}}\, ds}_{\left\langle \boldsymbol{\phi}_{\mathbf{q}} \otimes \boldsymbol{\phi}_{\mathbf{q}} \right\rangle^{\mathrm{th}}} + \underbrace{2\int_0^t \int_0^t e^{(t-s)\boldsymbol{\Theta}_{\mathbf{q}}} \mathbf{B}^{\mathrm{a}}_{\mathbf{q}}\, e^{-|s-s'|/\tau_a} e^{(t-s')\boldsymbol{\Theta}^{\top}_{\mathbf{q}}}\, ds\, ds'}_{\left\langle \boldsymbol{\phi}_{\mathbf{q}} \otimes \boldsymbol{\phi}_{\mathbf{q}} \right\rangle^{\mathrm{a}}} \end{aligned} \tag{34}$$

In particular, the first term reproduces the thermal result (Eqs. (22)–(26)), while the second adds the contribution from the active noise.

1 Active-noise contribution. From Eqs. (33) and (31), with thermal and active forces uncorrelated, the active part of the covariance is

$$\left\langle \boldsymbol{\phi}_{\mathbf{q}}(t) \otimes \boldsymbol{\phi}_{\mathbf{q}}(t) \right\rangle^{\mathrm{a}} = \int_0^t \int_0^t e^{(t-s)\boldsymbol{\Theta}_{\mathbf{q}}}\, 2\mathbf{B}^{\mathrm{a}}_{\mathbf{q}}\, e^{-|s-s'|/\tau_a}\, e^{(t-s')\boldsymbol{\Theta}^{\top}_{\mathbf{q}}}\, ds\, ds' \tag{35}$$

We denote steady-state value, i.e., value in the stationary limit ($t \to \infty$), of any quantity $(\cdot)$ in the presence of active noise by $(\cdot)_{\mathrm{ss}}$. Letting $u = t - s$, $v = t - s'$ gives

$$\begin{aligned} \mathbf{P}^{\mathrm{a}}_{\mathbf{q}} &:= \lim_{t\to\infty} \left\langle \boldsymbol{\phi}_{\mathbf{q}}(t) \otimes \boldsymbol{\phi}_{\mathbf{q}}(t) \right\rangle^{\mathrm{a}}_{\mathrm{ss}} \\ &= 2\int_0^{\infty} \int_0^{\infty} e^{u\boldsymbol{\Theta}_{\mathbf{q}}}\, \mathbf{B}^{\mathrm{a}}_{\mathbf{q}}\, e^{-|u-v|/\tau_a}\, e^{v\boldsymbol{\Theta}^{\top}_{\mathbf{q}}}\, du\, dv \end{aligned} \tag{36}$$

In parallel with Eq. (28), we show that the active-noise spectrum $\mathbf{P}^{\mathrm{a}}_{\mathbf{q}}$ satisfies the Sylvester–Lyapunov equation (with $\mathbf{I}$ denoting the identity matrix):

$$\begin{aligned} &\boldsymbol{\Theta}_{\mathbf{q}}\, \mathbf{P}^{\mathrm{a}}_{\mathbf{q}} + \mathbf{P}^{\mathrm{a}}_{\mathbf{q}}\, \boldsymbol{\Theta}^{\top}_{\mathbf{q}} = 2\,\mathbf{C}, \\ &\mathbf{C} = \left(\boldsymbol{\Theta}_{\mathbf{q}} - \frac{1}{\tau_a}\mathbf{I} \right)^{-1} \mathbf{B}^{\mathrm{a}}_{\mathbf{q}} + \mathbf{B}^{\mathrm{a}}_{\mathbf{q}} \left(\boldsymbol{\Theta}^{\top}_{\mathbf{q}} - \frac{1}{\tau_a}\mathbf{I} \right)^{-1} \end{aligned} \tag{37}$$

For diagonal $\mathbf{B}^{\mathrm{a}}_{\mathbf{q}}$ (cf. Eq. (32)), Eq. (37) can be solved in closed-form.

The active-noise contribution in Eq. (36) can be split into two regions $u \geq v$ and $v \geq v$

$$\mathbf{P}^{\mathrm{a}}_{\mathbf{q}} = 2(\mathbf{X}_1 + \mathbf{X}_2) \tag{38}$$

with

$$\mathbf{X}_1 = \int_0^{\infty} \int_0^{u} e^{u\boldsymbol{\Theta}_{\mathbf{q}}} \mathbf{B}^{\mathrm{a}}_{\mathbf{q}} e^{-(u-v)/\tau_a} e^{v\boldsymbol{\Theta}^{\top}_{\mathbf{q}}}\, dv\, du \tag{39}$$

and

$$\mathbf{X}_2 = \int_0^{\infty} \int_0^{v} e^{u\boldsymbol{\Theta}_{\mathbf{q}}} \mathbf{B}^{\mathrm{a}}_{\mathbf{q}} e^{(u-v)/\tau_a} e^{v\boldsymbol{\Theta}^{\top}_{\mathbf{q}}}\, du\, dv \tag{40}$$

We first compute $\mathbf{X}_1$, and we change variables $s = u - v$ and keep v as the second integration variable, so that $u = v + s$, $s \in [0, \infty)$, and $du\, dv = ds\, dv$. This gives

$$\begin{aligned} \mathbf{X}_1 &= \int_0^{\infty} \int_0^{\infty} e^{(v+s)\boldsymbol{\Theta}_{\mathbf{q}}} \mathbf{B}^{\mathrm{a}}_{\mathbf{q}}\, e^{-s/\tau_a}\, e^{v\boldsymbol{\Theta}^{\top}_{\mathbf{q}}}\, ds\, dv \\ &= \int_0^{\infty} e^{v\boldsymbol{\Theta}_{\mathbf{q}}} \left[\int_0^{\infty} e^{s\left(\boldsymbol{\Theta}_{\mathbf{q}} - \mathbf{I}/\tau_a\right)}\, ds \right] \mathbf{B}^{\mathrm{a}}_{\mathbf{q}} e^{v\boldsymbol{\Theta}^{\top}_{\mathbf{q}}}\, dv \\ &= -\int_0^{\infty} e^{v\boldsymbol{\Theta}_{\mathbf{q}}} \left(\boldsymbol{\Theta}_{\mathbf{q}} - \frac{1}{\tau_a}\mathbf{I} \right)^{-1} \mathbf{B}^{\mathrm{a}}_{\mathbf{q}} e^{v\boldsymbol{\Theta}^{\top}_{\mathbf{q}}}\, dv \end{aligned} \tag{41}$$

Similar calculations can be applied on $\mathbf{X}_2$. Then,

$$\mathbf{X}_2 = -\int_0^{\infty} e^{u\boldsymbol{\Theta}_{\mathbf{q}}} \mathbf{B}^{\mathrm{a}}_{\mathbf{q}} \left(\boldsymbol{\Theta}^{\top}_{\mathbf{q}} - \frac{\mathbf{I}}{\boldsymbol{\tau}_a} \right)^{-1} e^{u\boldsymbol{\Theta}^{\top}_{\mathbf{q}}}\, du \tag{42}$$

Adding $\mathbf{X}_1$ and $\mathbf{X}_2$ and relabeling the dummy integration variables u, $v \to t$, the active contribution becomes

$$\mathbf{P}^{\mathrm{a}}_{\mathbf{q}} = \int_0^{\infty} e^{t\boldsymbol{\Theta}_{\mathbf{q}}} \mathbf{D}_{\mathbf{q}} e^{t\boldsymbol{\Theta}_{\mathbf{q}}{}^{\top}}\, dt \tag{43}$$

where $\mathbf{D}_{\mathbf{q}}$ is defined as

$$\mathbf{D}_{\mathbf{q}} = -2\left(\boldsymbol{\Theta}_{\mathbf{q}} - \frac{1}{\tau_a}\mathbf{I} \right)^{-1} \mathbf{B}^{\mathrm{a}}_{\mathbf{q}} - 2\mathbf{B}^{\mathrm{a}}_{\mathbf{q}} \left(\boldsymbol{\Theta}^{\top}_{\mathbf{q}} - \frac{1}{\tau_a}\mathbf{I} \right)^{-1} \tag{44}$$

We now reduce this integral form to an equivalent Sylvester/Lyapunov equation. We define a function as

$$\begin{aligned} &\mathbf{F}(t) := e^{t\boldsymbol{\Theta}_{\mathbf{q}}} \mathbf{D}_{\mathbf{q}} e^{t\boldsymbol{\Theta}_{\mathbf{q}}{}^{\top}} \\ &\frac{d\mathbf{F}}{dt} = \boldsymbol{\Theta}_{\mathbf{q}} e^{t\boldsymbol{\Theta}_{\mathbf{q}}} \mathbf{D}_{\mathbf{q}} e^{t\boldsymbol{\Theta}^{\top}_{\mathbf{q}}} + e^{t\boldsymbol{\Theta}_{\mathbf{q}}} \mathbf{D}_{\mathbf{q}} e^{t\boldsymbol{\Theta}^{\top}_{\mathbf{q}}} \boldsymbol{\Theta}^{\top}_{\mathbf{q}} \end{aligned} \tag{45}$$

Integrating this from $t = 0$ to $t = \infty$ and using the definition of $\mathbf{P}^{\mathrm{a}}_{\mathbf{q}}$ gives

$$\begin{aligned} \int_0^{\infty} \frac{d\mathbf{F}}{dt}\, dt &= \mathbf{F}(t)\big|_0^{\infty} \\ \boldsymbol{\Theta}_{\mathbf{q}} P^{\mathrm{a}}_{\mathbf{q}} + \mathbf{P}^{\mathrm{a}}_{\mathbf{q}} \boldsymbol{\Theta}^{\top}_{\mathbf{q}} &= -\mathbf{D}_{\mathbf{q}} \end{aligned} \tag{46}$$

Substituting $\mathbf{D_q}$ gives

$$\mathbf{\Theta_q}\,\mathbf{P_q^a} + \mathbf{P_q^a}\,\mathbf{\Theta_q^\top} = -2\left(\mathbf{\Theta_q} - \frac{1}{\tau_a}\mathbf{I}\right)^{-1}\mathbf{B_q^a} - 2\mathbf{B_q^a}\left(\mathbf{\Theta_q^\top} - \frac{1}{\tau_a}\mathbf{I}\right)^{-1} \tag{47}$$

Defining the right-hand side as $2\mathbf{C_q}$, we recover the Sylvester/Lyapunov equation stated in Eq. (37).

2 Total fluctuation spectrum. Combining the thermal part (Eqs. (22)–(26)) with Eq. (36), the stationary covariance with both noises is

$$\mathbf{P_q^{th,a}} = \mathbf{P_q^{th}} + \mathbf{P_q^a} = \begin{bmatrix} \langle|\gamma_\mathbf{q}|^2\rangle_{ss}^{th,a} & \langle\gamma_\mathbf{q}\xi_\mathbf{q}\rangle_{ss}^{th,a} \\ \langle\gamma_\mathbf{q}\xi_\mathbf{q}\rangle_{ss}^{th,a} & \langle|\xi_\mathbf{q}|^2\rangle_{ss}^{th,a} \end{bmatrix} \tag{48}$$

In particular, for the strain component,

$$\langle|\gamma_\mathbf{q}|^2\rangle_{ss}^{th,a} = \langle|\gamma_\mathbf{q}|^2\rangle_{eq}^{th} + \langle|\gamma_\mathbf{q}|^2\rangle_{ss}^{a} \tag{49}$$

where $\langle|\gamma_\mathbf{q}|^2\rangle_{eq}^{th}$ is the thermal contribution given in Eq. (26) and $\langle|\gamma_\mathbf{q}|^2\rangle_{ss}^{a}$ is the active contribution in steady-state given in Eq. (55).

3.2 Free Energy. We now formulate an effective free energy of a living cell aggregate by incorporating the effects of fluctuations. The nonlinear Hamiltonian derived in the previous section implies that fluctuations in the strain field renormalize the macroscopic mechanical and electromechanical properties of the aggregate. Following the statistical mechanics coarse-graining procedure developed in Ref. [40], we define an effective free energy functional for the spatially uniform mean fields $(\bar{\gamma}, \bar{\xi})$, obtained after averaging over the fluctuations.

For the thermal case, the resulting effective free energy density is given by

$$\frac{1}{A}F^{\text{eff}}(\bar{\gamma},\bar{\xi}) = \left(\mu_2^{\text{eff}} + K(\bar{\xi}-\xi^*)\right)2\bar{\gamma}^2 + 4\mu_4^{\text{eff}}\bar{\gamma}^4 + \frac{8\mu}{\bar{\gamma}^{*2}}\bar{\gamma}^6 + \frac{\epsilon}{2\lambda^2}(\bar{\xi}-\xi^*)^2 + Q^{\text{eff}}(\bar{\xi}-\xi^*) \tag{50}$$

where the coefficients $\mu_2^{\text{eff}}, \mu_4^{\text{eff}}$, and Q^{eff} are fluctuation-renormalized effective parameters arising from thermal strain fluctuations. These are expressed in terms of the real-space mean-square strain fluctuation $\langle|\gamma|^2\rangle_{eq}^{th}$ [40]

$$\begin{aligned}(\mu_2^{\text{eff}})^{\text{th}} &= \mu\left(1 - \frac{16}{\gamma^*}\langle|\gamma|^2\rangle\right)_{eq}^{th} \\ (\mu_4^{\text{eff}})^{\text{th}} &= \frac{2\mu}{\gamma^*}\left(-1 + \frac{9}{\gamma^*}\langle|\gamma|^2\rangle\right)_{eq}^{th} \\ (Q^{\text{eff}})^{\text{th}} &= 2K\langle|\gamma|^2\rangle_{eq}^{th}\end{aligned} \tag{51}$$

In a true nonequilibrium active system, a thermodynamic free energy is not strictly defined. We use an instantaneous, energy-like functional whose coefficients incorporate both thermal and active contributions serving as an effective free energy for the coarse-grained system. To include active noise, we replace the thermal fluctuation spectrum $\langle|\gamma|^2\rangle_{eq}^{th}$ in Eq. (51) by the steady-state strain fluctuation spectrum $\langle|\gamma|^2\rangle_{ss}^{th,a}$, which accounts for both thermal and active contributions as given in Eq. (49). Thus, the effective free energy of a cell aggregate in the presence of both thermal and active becomes:

$$\frac{1}{A}(F^{\text{eff}})^{\text{th,a}}(\bar{\gamma},\bar{\xi}) = \left((\mu_2^{\text{eff}})^{\text{th,a}} + K(\bar{\xi}-\xi^*)\right)2\bar{\gamma}^2 + 4(\mu_4^{\text{eff}})^{\text{th,a}}\bar{\gamma}^4 + \frac{8\mu}{\bar{\gamma}^{*2}}\gamma^6 + \frac{\epsilon}{2\lambda^2}(\bar{\xi}-\xi^*)^2 + (Q^{\text{eff}})^{\text{th,a}}(\bar{\xi}-\xi^*) \tag{52}$$

with the renormalized effective coefficients as

$$\begin{aligned}(\mu_2^{\text{eff}})^{\text{th,a}} &= \mu\left(1 - \frac{16}{\gamma^*}\langle|\gamma|^2\rangle\right)_{ss}^{th,a} \\ (\mu_4^{\text{eff}})^{\text{th,a}} &= \frac{2\mu}{\gamma^*}\left(-1 + \frac{9}{\gamma^*}\langle|\gamma|^2\rangle\right)_{ss}^{th,a} \\ (Q^{\text{eff}})^{\text{th,a}} &= 2K\langle|\gamma|^2\rangle)_{ss}^{th,a}\end{aligned} \tag{53}$$

4 Results and Discussion

To investigate how active and thermal fluctuations impact the mechanical and electrical behavior of living tissues, we consider physiologically realistic model parameters informed by experimental data. Table 1 summarizes the chosen values for key physical quantities.

In the full electromechanical Hamiltonian, interaction terms involving J^{elas} and J^{elec} represent nonlocal couplings due to mechanical and electrical interactions across the tissue. However, for our parameter regime, these contributions are significantly smaller than the local elastic and electrostatic terms. Hence, we simplify the analysis by neglecting the terms involving J^{elas} and J^{elec}, focusing only on local behavior. With this local approximation, the thermal strain fluctuation spectrum (Eq. (26)) reduces to

$$\left\langle\left|\gamma_\mathbf{q}\right|^2\right\rangle_{eq}^{th} = \frac{\frac{K_BT}{L^3}\left(\frac{\epsilon}{\lambda^2}\right)}{(2Q_1)\left(\frac{\epsilon}{\lambda^2}\right) - 16K^2\bar{\gamma}^2} \tag{54}$$

The active contribution $\langle|\gamma_\mathbf{q}|^2\rangle_{ss}^{a}$ is obtained from the stationary covariance $\mathbf{P_q^a}$ derived in Sec. 3, by solving the associated Sylvester/Lyapunov equation using Eq. (A5) in Appendix. We get the active fluctuations for strain

$$\langle|\gamma_\mathbf{q}|^2\rangle_{ss}^{a} = \frac{2B_1\tau_a(1-\Theta_{22})\tau_a}{(\Theta_{11}+\Theta_{22})\left[1-(\Theta_{11}+\Theta_{22})\tau_a + (\Theta_{11}\Theta_{22}-\Theta_{12}\Theta_{21})\tau_a^2\right]} \tag{55}$$

Here, $\mathbf{\Theta}_{ij}$ are the entries in the matrix $\mathbf{\Theta_q}$ defined in Eq. (19).

To compute renormalized material properties in Eq. (53), the fluctuation spectrum in Fourier space must be converted to real-space quantities. This is achieved by integrating the spectrum over biologically motivated wavevector cutoffs. The lower cutoff $q_{\min} = 2\pi/t$ corresponds to the tissue scale, while the upper cutoff $q_{\max} = 2\pi/c$ corresponds to the cell scale, with typical values $t = 1$ mm and $c = 0.1\,\mu$m [49].

To capture the dissipative dynamics of strain and potential fields, we adopt a diagonal dissipation kernel inspired by prior work on

Table 1 Numerical values of the model parameters

Parameter	Value
Resting membrane potential of the cell(ξ^*)	−60 mV [43,44]
Range of potential variation of the cell $(\bar{\xi}-\xi^*)$	[−200 mV, 200 mV] [44–47]
Membrane thickness of the cell (λ)	5 nm [48]
Length of the cell membrane (L)	10 μm [48]
Shear modulus of the cell (μ)	200 Pa [49]
Electromechanical coupling constant (K)	$\sim 0.1\,\mu/\lvert\xi^*\rvert$
Effective resistance of the cell (R)	145 MΩ [50]
Characteristic time scale for active protein force noise (τ_a)	0.5 μs [49]
Viscosity of embedding fluid (η_0)	2.0×10^{-3} Pa s [51]
Dielectric permittivity (ϵ)	$20\epsilon_0$ F/m [48,52]
Vacuum permittivity (ϵ_0)	8.85×10^{-12} F/m
Boltzmann constant (k_B)	1.38×10^{-23} J/K
Temperature (T)	310 K

active membranes and active matter [26,53]. The kernel takes the form:

$$\Lambda_{\mathbf{q}} = \begin{bmatrix} \frac{1}{4\pi\eta_0} & 0 \\ 0 & \frac{1}{aRC} \end{bmatrix} \tag{56}$$

where η_0 represents the viscosity of the extracellular fluid, $a = 1/((\epsilon - \epsilon_0)\lambda)$ is the electrical constant of the cell membrane, R is an effective electrical resistance, and C is the capacitance of the cell membrane. This form captures the anisotropic relaxation dynamics of mechanical and electrical fields and is analytically tractable.

4.1 Renormalized Resting Potential. The local equilibrium state of the cell aggregate is determined by minimizing the effective free energy, which incorporates the effects of both thermal and active fluctuations.

To identify the equilibrium configuration, we use the principle of minimum free energy:

$$\begin{aligned} &\min_{(\gamma,\xi)} (F^{\text{eff}})^{\text{th,a}}(\gamma, \xi) \\ &\frac{\partial}{\partial\gamma}(F^{\text{eff}})^{\text{th,a}} = 0 \quad \text{and} \quad \frac{\partial}{\partial\xi}(F^{\text{eff}})^{\text{th,a}} = 0 \end{aligned} \tag{57}$$

The local small-strain minimizer is given by

$$(\gamma, \xi) = (0, \xi^{*\text{eff}}), \quad \xi^{*\text{eff}} = \xi^* - \frac{(Q^{\text{eff}})^{\text{th,a}}\lambda^2}{\epsilon} = \xi^* - \frac{2K\lambda^2}{\epsilon}\langle|\gamma|^2\rangle_{\text{ss}}^{\text{th,a}} \tag{58}$$

4.2 Solid-to-Fluid Phase Transition. The above framework enables us to quantify how fluctuations modify the mechanical phase behavior of cell aggregates—specifically, the transition between a *solid-like* phase (stable zero-strain state) and a *fluid-like* phase.

We identify a fluctuation-driven transition by the loss of stability of the small-strain local minimizer of the effective free energy (58). In our setting, the critical point is defined by the vanishing second derivative at the zero-strain state:

$$\begin{aligned} &\frac{\partial^2}{\partial\gamma^2}(F^{\text{eff}})^{\text{th,a}}\Big|_{(\gamma,\xi)=(0,\ \xi^{*\text{eff}})} = 0 \iff \\ &(\mu_2^{\text{eff}})^{\text{th,a}} + K\left(\xi^{*\text{eff}} - \xi^*\right) = 0 \end{aligned} \tag{59}$$

Using Eqs. (53) and (58), the corresponding critical mean-square strain is

$$\langle|\gamma|^2\rangle_{\text{ss,cr}}^{\text{th,a}} = \frac{\gamma^*}{16}\left(1 + \frac{K^2\lambda^2\gamma^*}{8\,\epsilon\,\mu}\right)^{-1} \tag{60}$$

For fluctuation strengths above (60), the zero-strain configuration loses stability and the aggregate transitions to a fluid-like state.

Moreover, living cells are capable of regulating their transmembrane potentials. In the present scenario with electromechanical coupling, tissues can actively regulate their stiffness and solid-to-fluid transition by manipulating their electric potentials. This capability allows them to adaptively respond to varying environmental conditions and physiological demands. By Eq. (52), we find the apparent shear modulus as

$$\begin{aligned} \mu^{\text{apparent}} &= \frac{\partial^2}{\partial\gamma^2}(F^{\text{eff}})^{\text{th,a}}|_{\gamma=0} \\ &= (\mu_2^{\text{eff}})^{\text{th,a}} + K(\xi - \xi^*) \\ &= \mu\left(1 - \frac{16}{\gamma^*}\langle|\gamma|^2\rangle\right)_{\text{ss}}^{\text{th,a}} + K(\xi - \xi^*) \end{aligned} \tag{61}$$

When $\mu^{\text{apparent}} = 0$, the system loses mechanical rigidity, consistent with the onset of fluid-like behavior. Solving this equation yields the critical fluctuation at any prescribed applied electric potential ξ:

$$\langle|\gamma|^2\rangle_{\text{ss}}^{\text{th,a}} = \frac{\gamma^*}{16}\left[1 + \frac{K}{\mu}(\xi - \xi^*)\right] \tag{62}$$

Figure 2 shows the phase boundary for solid–fluid-like transitions computed using representative physiological values. The curve separates the stable (solid-like) region, where $\gamma = 0$ is a local minimum, from the unstable (fluid-like) region. As fluctuations increase or the average potential ξ increases, the tissue softens and enters a fluid-like state.

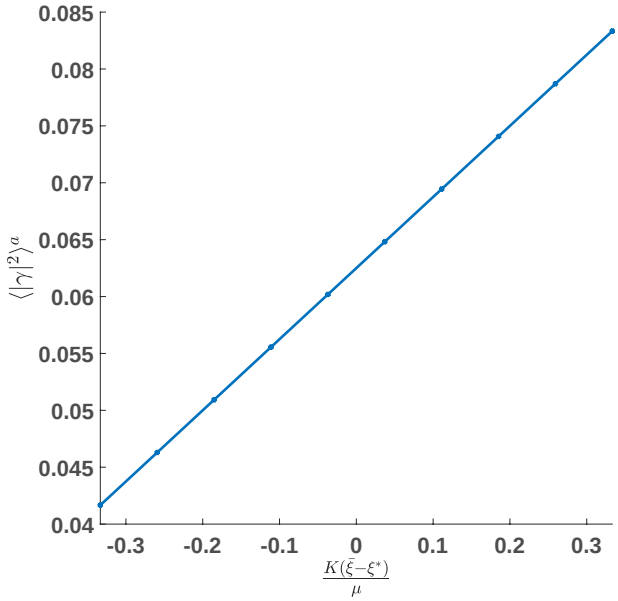

Fig. 2 Phase diagram for solid-to-fluid phase transition in cell aggregates. For chosen numerical values in this work, the range of nondimensional *x*-axis corresponds to the range of change in electric potential as $(\xi - \xi^*) \in [-200\,\text{mV}, 200\,\text{mV}]$ and *y*-axis as the ensemble average of fluctuations in strain.

4.3 Electromechanical Responses. The coupling between electric potential and mechanical strain in our model enables us to study how cell aggregates respond to external stimuli, both electrical and mechanical. We explore this behavior through two primary perspectives:

(1) Stress–strain (elastic) response under applied mechanical stress
(2) Strain response under applied electric potential (inverse piezoelectric-like effect)

We first examine how external shear stress σ^e modifies the mechanical response of the aggregate at the renormalized potential $\bar{\xi} = \xi^{*\text{eff}}$. The equilibrium shear strain γ^{eq} minimizes the effective energy including external work:

$$\gamma^{\text{eq}} = \text{argmin}_\gamma\left(\frac{1}{A}(F^{\text{eff}})^{\text{th,a}}(\gamma, \bar{\xi}) - 2\sigma^e\gamma\right) \tag{63}$$

This leads to the stationary condition:

$$4\gamma\left((\mu_2^{\text{eff}})^{\text{th,a}} + K(\bar{\xi} - \xi^*)\right) + 16(\mu_4^{\text{eff}})^{\text{th,a}}\gamma^3 + \frac{48\mu}{\gamma^{*2}}\gamma^4 - 2\sigma^e = 0 \tag{64}$$

This is a nonlinear algebraic equation in γ whose solution gives the equilibrium strain. Figure 3 plots σ^e versus γ^{eq} for several values of active fluctuation strength $\langle|\gamma|^2\rangle_{\text{eq}}^{\text{th,a}}$. It shows that for

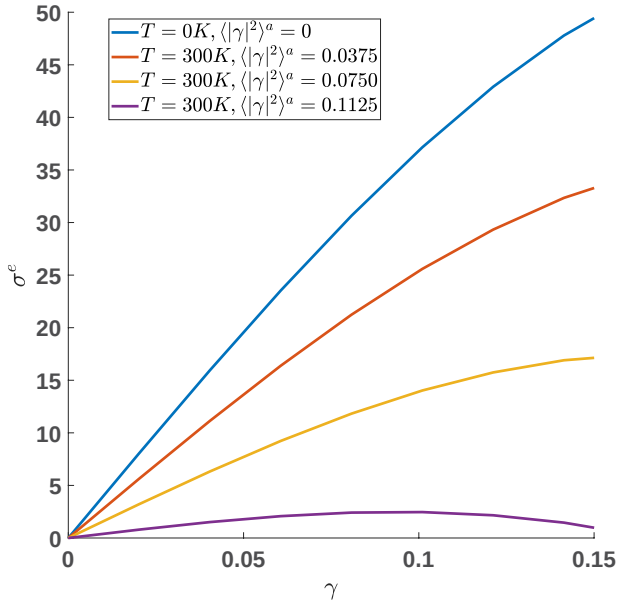

Fig. 3 Mechanical response of a cell aggregate with applied potential $\bar{\xi} = \xi^{*\text{eff}}$.

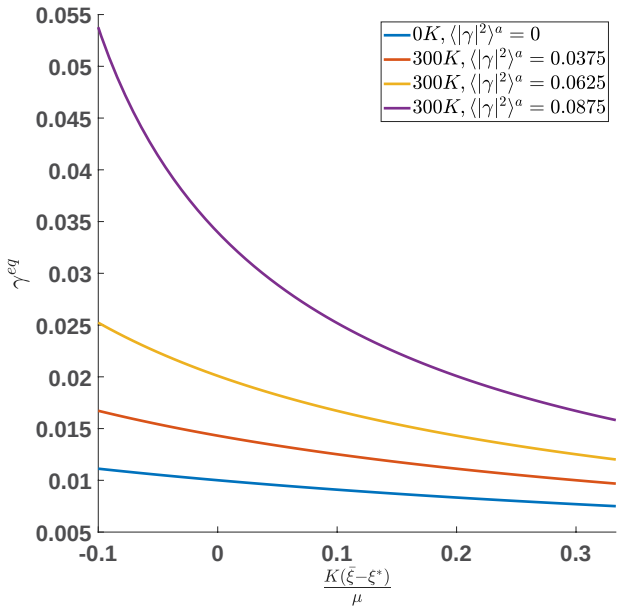

Fig. 4 Macroscopic inverse piezoelectric-like response of cell aggregate. Equilibrium shear strain γ^{eq} is plotted against normalized electric potential along *x*-axis. For chosen numerical values in this work, the range of non-dimensionlized *x*-axis in plot corresponds to the range of change in electric potential as $(\bar{\xi} - \xi^*) \in [-200\,\text{mV}, 200\,\text{mV}]$.

low fluctuation values (below the critical value), the cell aggregate behaves like a solid, with a stiff and nonlinear response and for fluctuation strengths above the critical threshold, the system behaves like a fluid, with a soft and more compliant response.

Next, we fix the external stress σ^e (e.g., $\sigma^e = 0.02\mu$) and vary the applied electric potential $\bar{\xi}$ to study how the electromechanical coupling induces strain. For each value of $\bar{\xi}$, we compute γ^{eq} by solving the same minimization condition in Eq. (63).

Figure 4 shows the resulting strain γ^{eq} plotted against the normalized potential $K(\bar{\xi} - \xi^*)/\mu$ for different levels of fluctuation strength of the strain. This emergent electromechanical behavior at macroscopic tissue length-scale does not require any piezoelectric material properties at the cellular scale.

5 Concluding Remarks

The findings presented here suggest that we must move beyond viewing living tissues as static structural scaffolds and instead recognize them as active, stochastic engines [2,3]. Our theoretical framework demonstrates that the coupling between electrical potential and mechanical strain is not just a secondary feature of cellular life; it is a fundamental driver of its physical state. By analytically showing how active noise renormalizes material properties, we have established a mechanistic bridge between the microscopic randomness of protein activity and the macroscopic fluidity of tissues [40].

In our view, fluctuations can be treated as tunable control parameters that allow biological systems to navigate between solid and fluid phases with exquisite precision. The prediction of emergent electromechanical responses, such as the macroscopic inverse piezoelectric-like effect, highlights how collective interactions can generate sophisticated material properties without the need for specialized microscopic prerequisites at the single-cell level. This approach potentially opens new avenues for exploring how biological patterning and morphogenesis arise not in spite of fluctuations, but because of them.

Acknowledgment

The author PS acknowledges support from the Cullen Professorship of the University of Houston.

Conflict of Interest

There are no conflicts of interest.

Data Availability Statement

The authors attest that all data for this study are included in the article.

Appendix: Closed-Form Evaluation of Integral

Let $\tau > 0$, $\mathbf{B} \in \mathbb{R}^{d\times d}$, and $\mathbf{A} \in \mathbb{R}^{d\times d}$ be a square matrix whose eigenvalues all have strictly negative real parts (Eq. (36)). Then, the integral

$$\mathbf{X} =: \int_0^\infty \int_0^\infty e^{u\mathbf{A}}\, \mathbf{B}\, e^{-|u-v|/\tau}\, e^{v\mathbf{A}^\top}\, du\, dv \tag{A1}$$

is well-defined and solves the Sylvester–Lyapunov equation:

$$\mathbf{A}\mathbf{X} + \mathbf{X}\mathbf{A}^\top = \left(\mathbf{A} - \frac{1}{\tau}\mathbf{I}\right)^{-1} \mathbf{B} + \mathbf{B}\left(\mathbf{A} - \frac{1}{\tau}\mathbf{I}\right)^{-\top}$$

To see this, we split the integral on the right-hand side of Eq. (A1) into the two regions $u \geq v$ and $v \geq u$:

$$\mathbf{X} = \int_0^\infty \int_0^u e^{u\mathbf{A}} \mathbf{B}\, e^{-(u-v)/\tau} e^{v\mathbf{A}^\top}\, dv\, du + \int_0^\infty \int_0^v e^{u\mathbf{A}} \mathbf{B}\, e^{-(v-u)/\tau} e^{v\mathbf{A}^\top}\, du\, dv$$
$$=: \mathbf{X}_1 + \mathbf{X}_2$$

For $\mathbf{X}_1$, set $s = u - v \geq 0$ so that $u = v + s$ and $du = ds$, giving

$$\mathbf{X}_1 = \int_0^\infty \int_0^\infty e^{(v+s)\mathbf{A}} \mathbf{B} e^{-s/\tau} e^{v\mathbf{A}^\top}\, ds\, dv = \int_0^\infty e^{v\mathbf{A}} \left(\int_0^\infty e^{s(\mathbf{A} - \frac{1}{\tau}\mathbf{I})}\, ds \right) \mathbf{B} e^{v\mathbf{A}^\top}\, dv$$

Since eigenvalues of $\mathbf{A}-(1/\tau)\mathbf{I}$ all have negative real parts, $\int_0^\infty e^{s(\mathbf{A}-(1/\tau)\mathbf{I})}ds = -(\mathbf{A}-(1/\tau)\mathbf{I})^{-1}$, hence

$$\mathbf{X}_1 = \int_0^\infty e^{v\mathbf{A}}\left(-(\mathbf{A}-\frac{1}{\tau}\mathbf{I})^{-1}\mathbf{B}\right)e^{v\mathbf{A}^\top}\,dv \tag{A2}$$

Differentiating the integrands of $\mathbf{X}_1$ and $\mathbf{X}_2$ and integrating from 0 to ∞, we conclude that

$$\mathbf{A}\mathbf{X}_1+\mathbf{X}_1\mathbf{A}^\top = \left(\mathbf{A}-\frac{1}{\tau}\mathbf{I}\right)^{-1}\mathbf{B}, \quad \mathbf{A}\mathbf{X}_2+\mathbf{X}_2\mathbf{A}^\top = \mathbf{B}\left(\mathbf{A}-\frac{1}{\tau}\mathbf{I}\right)^{-\top}$$

Let $\mathbf{X} := \mathbf{X}_1+\mathbf{X}_2$. Adding the two identities yields the Sylvester–Lyapunov equation:

$$\mathbf{A}\mathbf{X}+\mathbf{X}\mathbf{A}^\top = \mathbf{C} := \left(\mathbf{A}-\frac{1}{\tau}\mathbf{I}\right)^{-1}\mathbf{B}+\mathbf{B}\left(\mathbf{A}^\top-\frac{1}{\tau}\mathbf{I}\right)^{-\top} \tag{A3}$$

Moreover, suppose that $\mathbf{A}$ is diagonalizable:

$$\mathbf{A} = \mathbf{V}\mathbf{\Lambda}\mathbf{V}^{-1}, \quad \mathbf{\Lambda} = \mathrm{diag}(\lambda_1,\ldots,\lambda_d), \quad \lambda_i<0$$

Set

$$\mathbf{Y} := \mathbf{V}^{-1}\mathbf{X}\mathbf{V}^{-\top}, \quad \mathbf{D} := \mathbf{V}^{-1}\mathbf{C}\mathbf{V}^{-\top}$$

Then, Eq. (A3) becomes

$$\mathbf{\Lambda}\mathbf{Y}+\mathbf{Y}\mathbf{\Lambda}^\top = \mathbf{D}$$

hence entrywise

$$(\lambda_i+\lambda_j)\,Y_{ij} = D_{ij} \quad\Longrightarrow\quad Y_{ij} = \frac{D_{ij}}{\lambda_i+\lambda_j} \quad (1\le i,j\le d) \tag{A4}$$

provided $\lambda_i+\lambda_j\neq 0$. Therefore, the explicit solution is given by

$$\mathbf{X} = \mathbf{V}\mathbf{Y}\mathbf{V}^\top, \quad Y_{ij} = \frac{\left(\mathbf{V}^{-1}\mathbf{C}\mathbf{V}^{-\top}\right)_{ij}}{\lambda_i+\lambda_j} \tag{A5}$$

References

[1] Ramesh, S., Purohit, P. K., and Kulkarni, Y., 2026, "A Tutorial on the Statistical Mechanics of Soft Active Matter," Appl. Mech. Rev., pp. 1–37.
[2] Bray, D., 2000, *Cell Movements: From Molecules to Motility*, Garland Science, New York.
[3] Alberts, B., Bray, D., Hopkin, K., Johnson, A. D., Lewis, J., Raff, M., Roberts, K., and Walter, P., 2015, *Essential Cell Biology*, Garland Science, New York.
[4] Ranade, S. S., Syeda, R., and Patapoutian, A., 2015, "Mechanically Activated Ion Channels," Neuron, **87**(6), pp. 1162–1179.
[5] Kung, C., 2005, "A Possible Unifying Principle for Mechanosensation," Nature, **436**(7051), pp. 647–654.
[6] Cox, C. D., Bavi, N., and Martinac, B., 2019, "Biophysical Principles of Ion-Channel-Mediated Mechanosensory Transduction," Cell Rep., **29**(1), pp. 1–12.
[7] Wozniak, M. A., and Chen, C. S., 2009, "Mechanotransduction in Development: A Growing Role for Contractility," Nat. Rev. Mol. Cell Biol., **10**(1), pp. 34–43.
[8] Andersson, M., Okeyo, G., Wilson, D., Keizer, H., Moe, P., Blount, P., Fine, D., Dodabalapur, A., and Duran, R. S., 2008, "Voltage-Induced Gating of the Mechanosensitive Mscl Ion Channel Reconstituted in a Tethered Lipid Bilayer Membrane," Biosens. Bioelectron., **23**(6), pp. 919–923.
[9] Harland, B., Brownell, W. E., Spector, A. A., and Sun, S. X., 2010, "Voltage-Induced Bending and Electromechanical Coupling in Lipid Bilayers," Phys. Rev. E: Stat., Nonlinear, Soft Matter Phys., **81**(3), p. 031907.
[10] Ingber, D. E., 2006, "Cellular Mechanotransduction: Putting All the Pieces Together Again," FASEB J., **20**(7), pp. 811–827.
[11] Bi, D., Lopez, J., Schwarz, J. M., and Manning, M. L., 2015, "A Density-Independent Rigidity Transition in Biological Tissues," Nat. Phys., **11**(12), pp. 1074–1079.
[12] Trepat, X., and Sahai, E., 2018, "Mesoscale Physical Principles of Collective Cell Organization," Nat. Phys., **14**(7), pp. 671–682.
[13] Heisenberg, C.-P., and Bellaïche, Y., 2013, "Forces in Tissue Morphogenesis and Patterning," Cell, **153**(5), pp. 948–962.
[14] Etournay, R., Popović, M., Merkel, M., Nandi, A., Blasse, C., Aigouy, B., Brandl, H., et al., 2015, "Interplay of Cell Dynamics and Epithelial Tension During Morphogenesis of the Drosophila Pupal Wing," Elife, **4**, p. e07090.
[15] Serra-Picamal, X., Conte, V., Vincent, R., Anon, E., Tambe, D. T., Bazellieres, E., Butler, J. P., Fredberg, J. J., and Trepat, X., 2012, "Mechanical Waves During Tissue Expansion," Nat. Phys., **8**(8), pp. 628–634.
[16] Sunyer, R., Conte, V., Escribano, J., Elosegui-Artola, A., Labernadie, A., Valon, L., Navajas, D., et al., 2016, "Collective Cell Durotaxis Emerges From Long-Range Intercellular Force Transmission," Science, **353**(6304), pp. 1157–1161.
[17] Turlier, H., Fedosov, D. A., Audoly, B., Auth, T., Gov, N. S., Sykes, C., Joanny, J.-F., Gompper, G., and Betz, T., 2016, "Equilibrium Physics Breakdown Reveals the Active Nature of Red Blood Cell Flickering," Nat. Phys., **12**(5), pp. 513–519.
[18] Prost, J., Jülicher, F., and Joanny, J.-F., 2015, "Active Gel Physics," Nat. Phys., **11**(2), pp. 111–117.
[19] Zwanzig, R., 2001, *Nonequilibrium Statistical Mechanics*, Oxford University Press, New York.
[20] Mitchel, J. A., Das, A., O'Sullivan, M. J., Stancil, I. T., DeCamp, S. J., Koehler, S., Ocaña, O. H., Butler, J. P., Fredberg, J. J., and Nieto, M. A., 2020, "In Primary Airway Epithelial Cells, the Unjamming Transition is Distinct From the Epithelial-to-Mesenchymal Transition," Nat. Commun., **11**(1), p. 5053.
[21] Mierke, C. T., 2025, "Ecm Mechanics Control Jamming-to-Unjamming Transition of Cancer Cells," Cells, **14**(13), p. 943.
[22] Zimmermann, J., Camley, B. A., Rappel, W.-J., and Levine, H., 2016, "Contact Inhibition of Locomotion Determines Cell–Cell and Cell–Substrate Forces in Tissues," Proc. Natl. Acad. Sci. U. S. A., **113**(10), pp. 2660–2665.
[23] Helfrich, W., 1973, "Elastic Properties of Lipid Bilayers: Theory and Possible Experiments," Z. Naturforschung c, **28**(11-12), pp. 693–703.
[24] Seifert, U., 1997, "Configurations of Fluid Membranes and Vesicles," Adv. Phys., **46**(1), pp. 13–137.
[25] Safran, S., 2018, *Statistical Thermodynamics of Surfaces, Interfaces, and Membranes*, CRC Press, Boca Raton, FL.
[26] Kulkarni, Y., 2023, "Fluctuations of Active Membranes With Nonlinear Curvature Elasticity," J. Mech. Phys. Solids, **173**, p. 105240.
[27] Sojib Kaisar, M., Hassan, R., Farokhirad, S., and Ahmadpoor, F., 2025, "Renormalization of Mechanical Properties in Fluctuating Active Membranes," ASME J. Appl. Mech., **92**(12), p. 121005.
[28] Ahmadpoor, F., and Sharma, P., 2016, "Thermal Fluctuations of Vesicles and Nonlinear Curvature Elasticity—Implications for Size-Dependent Renormalized Bending Rigidity and Vesicle Size Distribution," Soft Matter, **12**(9), pp. 2523–2536.
[29] Ramesh, S., and Kulkarni, Y., 2024, "Statistical Mechanics of Active Vesicles and the Size Distribution Paradox," J. Mech. Phys. Solids, **191**, p. 105749.
[30] Mathew, A., and Kulkarni, Y., 2025, "Active Matter as the Underpinning Agency for Extraordinary Sensitivity of Biological Membranes to Electric Fields," Proc. Natl. Acad. Sci. U. S. A., **122**(12), p. e2427255122.
[31] Ahmadpoor, F., Liu, L., and Sharma, P., 2015, "Thermal Fluctuations and the Minimum Electrical Field That Can Be Detected by a Biological Membrane," J. Mech. Phys. Solids, **78**, pp. 110–122.
[32] Ramesh, S., Purohit, P. K., and Kulkarni, Y., 2026, "On the Statistical Mechanics of Active Membranes: Some Selected Results," preprint arXiv:2602.19249.
[33] Ahmadpoor, F., and Sharma, P., 2015, "Flexoelectricity in Two-Dimensional Crystalline and Biological Membranes," Nanoscale, **7**(40), pp. 16555–16570.
[34] Torbati, M., Mozaffari, K., Liu, L., and Sharma, P., 2022, "Coupling of Mechanical Deformation and Electromagnetic Fields in Biological Cells," Rev. Mod. Phys., **94**(2), p. 025003.
[35] Liu, L., and Sharma, P., 2013, "Flexoelectricity and Thermal Fluctuations of Lipid Bilayer Membranes: Renormalization of Flexoelectric, Dielectric, and Elastic Properties," Phys. Rev. E: Stat., Nonlinear, Soft Matter Phys., **87**(3), p. 032715.
[36] Deserno, M., 2015, "Fluid Lipid Membranes: From Differential Geometry to Curvature Stresses," Chem. Phys. Lipids, **185**, pp. 11–45.
[37] Khandagale, P., Breitzman, T., Majidi, C., and Dayal, K., 2023, "Statistical Field Theory for Nonlinear Elasticity of Polymer Networks With Excluded Volume Interactions," Phys. Rev. E, **107**(6), p. 064501.
[38] Purohit, P. K., and Smith, D. H., 2016, "A Model for Stretch Growth of Neurons," J. Biomech., **49**(16), pp. 3934–3942.
[39] Grasinger, M., Majidi, C., and Dayal, K., 2021, "Nonlinear Statistical Mechanics Drives Intrinsic Electrostriction and Volumetric Torque in Polymer Networks," Phys. Rev. E, **103**(4), p. 042504.
[40] Khandagale, P., Lin, H., Liu, L., and Sharma, P., 2025, "Statistical Mechanics of Cell Aggregates: Explaining the Phase Transition and Paradoxical Piezoelectric Behavior of Soft Biological Tissues," Soft Matter, **21**(28), pp. 5655–5668.
[41] Irvine, K. D., and Wieschaus, E., 1994, "Cell Intercalation During Drosophila Germband Extension and Its Regulation by Pair-Rule Segmentation Genes," Development, **120**(4), pp. 827–841.
[42] Hespanha, J. P., 2018, *Linear Systems Theory*, Princeton University Press, Princeton, NJ.
[43] Heimburg, T., and Jackson, A. D., 2005, "On Soliton Propagation in Biomembranes and Nerves," Proc. Natl. Acad. Sci. U. S. A., **102**(28), pp. 9790–9795.
[44] Beyder, A., and Sachs, F., 2009, "Electromechanical Coupling in the Membranes of Shaker-Transfected Hek Cells," Proc. Natl. Acad. Sci. U. S. A., **106**(16), pp. 6626–6631.
[45] Antonov, V., Smirnova, E. Y., and Shevchenko, E., 1990, "Electric Field Increases the Phase Transition Temperature in the Bilayer Membrane of Phosphatidic Acid," Chem. Phys. Lipids, **52**(3–4), pp. 251–257.
[46] Heimburg, T., 2012, "The Capacitance and Electromechanical Coupling of Lipid Membranes Close to Transitions: The Effect of Electrostriction," Biophys. J., **103**(5), pp. 918–929.
[47] Mosgaard, L. D., Zecchi, K. A., and Heimburg, T., 2015, "Mechano-Capacitive Properties of Polarized Membranes," Soft Matter, **11**(40), pp. 7899–7910.

[48] Krichen, S., Liu, L., and Sharma, P., 2017, "Biological Cell as a Soft Magnetoelectric Material: Elucidating the Physical Mechanisms Underpinning the Detection of Magnetic Fields by Animals," Phys. Rev. E, **96**(4), p. 042404.

[49] Moeendarbary, E., and Harris, A. R., 2014, "Cell Mechanics: Principles, Practices, and Prospects," Wiley Interdiscipl. Rev. Syst. Biol. Med., **6**(5), pp. 371–388.

[50] Fish, R. M., and Geddes, L. A., 2009, "Conduction of Electrical Current to and Through the Human Body: A Review," Eplasty, **9**, p. e44.

[51] Bera, K., Kiepas, A., Godet, I., Li, Y., Mehta, P., Ifemembi, B., Paul, C. D., et al., 2022, "Extracellular Fluid Viscosity Enhances Cell Migration and Cancer Dissemination," Nature, **611**(7935), pp. 365–373.

[52] Stern, H. A., and Feller, S. E., 2003, "Calculation of the Dielectric Permittivity Profile for a Nonuniform System: Application to a Lipid Bilayer Simulation," J. Chem. Phys., **118**(7), pp. 3401–3412.

[53] Khandagale, P., Liu, L., and Sharma, P., 2025, "Flexoelectricity and the Fluctuations of (active) Living Cells: Implications for Energy Harvesting, Ion Transport, and Neuronal Activity," PNAS Nexus, **4**(12), p. 362.